



ORIGINAL ARTICLE

# The effects of nozzle diameter and length on the resulting strand properties for shotcrete 3D printing

Martin David · Niklas Freund · Klaus Dröder · Dirk Lowke

Received: 5 July 2023 / Accepted: 12 September 2023 / Published online: 28 September 2023  
© The Author(s) 2023

**Abstract** Additive manufacturing in construction (AMC) enables new design methods and strategies within the construction industry. In particular, Shotcrete 3D Printing (SC3DP) offers a high degree of design freedom by enabling the deposition of concrete at variable layer orientation based on a wet-mix shotcrete process. However, the mechanical properties and geometry of the printed layers are dependent on the material and process parameters used. In this context, the effects of air and concrete flow rates, path planning parameters, and material parameters have been investigated in previous research. The presented study investigates the influence of the nozzle geometry on the resulting strand properties, e.g. strand

geometry, layer bond strength, and compressive strength, to evaluate nozzle diameter and length as control parameters for the SC3DP process. Experimental investigations were performed with fixed nozzle diameters between 10 and 30 mm and nozzle lengths ranging from 100 to 200 mm. The results show a significant influence of the nozzle diameter on the resulting strand geometry as well as the mechanical properties. Finally, concepts for a nozzle with a controllable outlet diameter were developed and evaluated.

**Keywords** Additive manufacturing in construction · AMC · Shotcrete 3D Printing · SC3DP · Nozzle geometry

---

Martin David and Niklas Freund contributed equally to this work and share the first authorship.

---

M. David · K. Dröder

Institute of Machine Tools and Production Technology,  
Technische Universität Braunschweig, 38106 Brunswick,  
Germany

e-mail: m.david@tu-braunschweig.de

K. Dröder

e-mail: k.droeder@tu-braunschweig.de

N. Freund · D. Lowke

Institute of Building Materials, Concrete Construction and  
Fire Safety, Technische Universität Braunschweig,  
38106 Brunswick, Germany

e-mail: n.freund@ibmb.tu-bs.de

D. Lowke

e-mail: d.lowke@ibmb.tu-bs.de

## 1 Introduction

In order to address major challenges in construction, such as a low level of automation, a shortage of skilled labour, or high carbon emissions, research and industrial developments are focusing on automation approaches. Especially Additive Manufacturing in Construction (AMC) opens up possibilities for innovative design methods and building strategies for architects and civil engineers [1–3]. Hence, different additive manufacturing techniques are investigated, such as particle bed binding [4], material extrusion [5],



or material jetting [6]. A growing area of research focuses on the identification of suitable printing materials and process parameters for the production of geometrically precise components with sufficient properties, such as mechanical performance and durability [7–11].

Shotcrete 3D Printing (SC3DP) is an Additive Manufacturing (AM) technique based on a wet-mix shotcrete process. It is classified as a material jetting process [12] and is characterised by the deposition of material under the addition of pressurised air at the printing nozzle. Due to high application rates and a good layer bond strength, SC3DP offers great potential for the efficient production of large structural concrete elements [13]. By applying the material at a defined nozzle-to-strand-distance, SC3DP allows for an angled material deposition in overhangs (Fig. 1a). A wide range of process parameters are used within SC3DP to influence the geometry of the applied layers (see Fig. 1b). Small adjustments to the process parameters (e.g. concrete volume flow or air volume flow), material parameters (e.g. accelerator dosage), or path planning (e.g. nozzle-to-strand-distance) affect both the resulting layer geometry and the quality of the printed object (e.g. layer bond strength) [9–11, 14]. Therefore, in-depth research into the material-process-interaction is required to improve and establish material and process-related limits.

## 2 Control of strand geometry within shotcrete-based additive manufacturing—state of the art

Predicting and controlling the strand geometry is a key task in AM to translate the dimensions previously defined in the 3D digital model into the printing process. For example, for the extrusion of very stiff and unsheared material, the resulting geometry of the deposited strands depends, in particular, on the nozzle geometry [2]. In the extrusion of more flowable concrete, where the material is sheared before leaving the nozzle, the concrete spreads out depending on the material rheology (e.g. yield stress), forming the final layer geometry [2]. In general, nozzle speed, nozzle distance, and concrete volume flow must be coordinated to avoid under- or over-extrusion [5].

In SC3DP, the concrete is pumped to the nozzle in a dense stream and, unlike in extrusion or other AM processes, subsequently torn up into a jet using compressed air. When the concrete jet reaches the ground, the concrete builds up into a strand of material. This characteristic allows for greater nozzle distances and increases the robustness of the process with regard to under-and over “extrusion”. Thus, varying material application rates result primarily in different strand heights rather than in the formation of gaps or material accumulations in the strand. Within shotcrete-based AM, three main strategies for affecting the strand geometry have been investigated so far:

- (a) Process parameters
- (b) Material parameters
- (c) External tools

**Process parameters** in shotcrete-based AM include concrete and air volume flow, as well as path planning parameters such as nozzle-to-strand-distance and traverse speed. It was found that increasing the air volume flow results in a slight increase in width and a slight decrease in the height of the sprayed layers. Furthermore, Böhler et al. showed an increase in layer bond strength and concrete density with an increase in air volume flow. At high air pressures (3–5 bar), the formation of flatter and wider layers is visible [9, 14]. However, at low air pressures (0.5–1 bar), Liu et al. observed no significant effect on the strand geometry [15].

The increase in concrete volume flow results naturally in an increase in specimen cross-sectional area due to a higher material feed rate. Böhler et al. observed a significant increase in specimen height with a slight increase in its width as well as a slight decrease in layer bond strength while keeping all other parameters constant [14].

In terms of nozzle traverse speed (Fig. 2a), a decrease in height with a slight decrease in width is observed at increased traverse speeds [10]. This could be a result of a lower amount of material volume per running meter.

By increasing the nozzle-to-strand-distance (Fig. 2b), an increase in width and a decrease in height is achieved [10]. By increasing the nozzle-to-strand-distance, the particles in the shotcrete jet spread in a wider area and therefore increasing the sample width. Due to a constant material flow rate, the specimen height decreases.

As another possible path planning strategy, Kloft et al. suggested the concept of a rotating nozzle movement (Fig. 2c) [13]. This approach can be used to produce wider strands of material.

The effect of **material parameters** was investigated primarily for the utilisation of a shotcrete accelerator. The accelerator is added at the nozzle to increase the structural build-up of the material for higher vertical build rates [9–11, 14]. Furthermore, the addition of accelerator has a significant effect on the resulting geometry of the deposited layers. Increasing the accelerator dosage results in higher and narrower layers. However, high accelerator dosages show negative effects on the interlocking and bonding between the layers. This is particularly relevant during

breaks in the printing process, as the risk of cold joints between layers is increased, which would significantly reduce structural integrity. In addition to the acceleration of the material setting and hardening, the initial concrete composition is varied and therefore influences the material's rheological properties, which in turn affects the resulting layer geometry [16].

**External tools** such as guided trowels or slip-forms are further used to affect the geometry of 3D-printed parts. This technique is primarily used to smoothen the surface of the print and is already applied during the extrusion [17], as well as spraying techniques. To control the strand width, trowels can be placed on both sides of the strand. Depending on the desired layer geometry, the distance between the trowels is varied

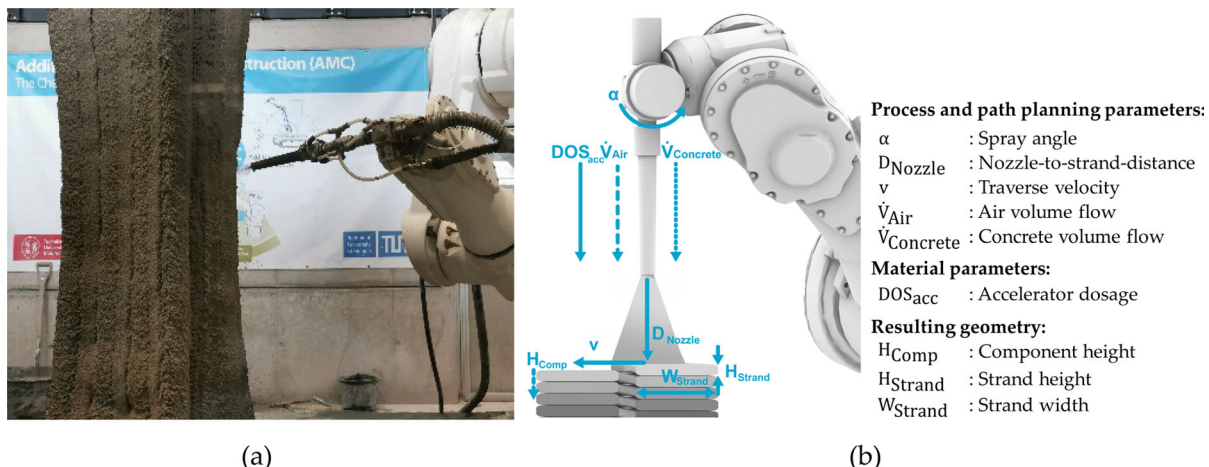


**Fig. 1** **a** Shotcrete 3D printed overhang (Credit: ITE TU BS), **b** Material- and process parameters within Shotcrete 3D Printing (modified from [10])

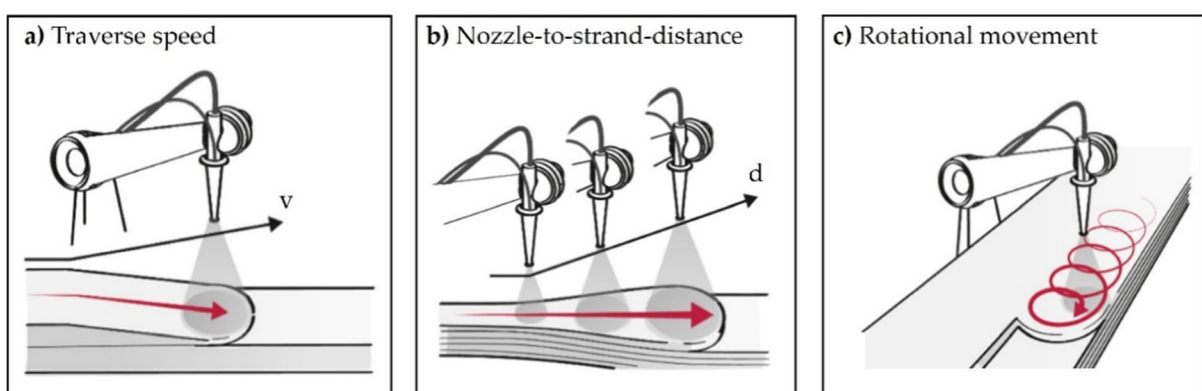


**Fig. 2** Affecting SC3D-printed layer geometry through adjustments of **a** Traverse speed  $v$ ; **b** Nozzle-to-strand-distance  $d$ , and **c** Rotational movements (modified from [13])

by an actuated linear axis [18]. In contrast to the previously described approaches, external tools only affect the strand geometry if enough material is deposited, which results in a less reliable approach for creating wider strands without modifications to the process and its parameters (e.g. concrete volume flow or traverse speed).

Each of the presented strategies must be evaluated regarding both the geometrical effect as well the influence on the resulting strand properties, such as the mechanical performance in order to qualify the process for industrial applications. A controlled variation in combination with sophisticated planning strategies will lead to high component qualities regarding geometry and material properties.

### 3 Experimental investigations: control of strand geometry by nozzle geometry in SC3DP

#### 3.1 Scope

As described in Chapter 2, several parameters can be adjusted to influence the strand geometry in SC3DP. As Galé et al. demonstrated the influence of the shotcrete nozzle design on the resulting material projection angle [19], the nozzle geometry itself has the potential to be used as a control parameter for SC3DP. Furthermore, an automated variation of the nozzle geometry during the printing process could be used to directly influence the strand geometry and mechanical strand properties. Therefore, the present study aims to answer the following research questions:

- How does a variation in nozzle outlet diameter ( $d_o$ ) and nozzle length ( $L$ ) affect the geometry and mechanical properties of deposited strands?

**Table 1** Properties of the nozzle geometries

Nozzle abbreviation	Length $L$ (mm)	Inlet diameter $d_i$ (mm)	Outlet diameter $d_o$ (mm)	Nozzle angle $\alpha$ (°)	Type of shape
n_200_10	200	25	10	2.15	Tapered
n_200_15	200	25	15	1.43	Tapered
n_200_20	200	25	20	0.72	Tapered
n_100_20	100	25	20	1.43	Tapered
n_150_20	150	25	20	0.95	Tapered
n_200_25	200	25	25	0.00	Straight
n_200_30	200	25	30	– 0.72	Widened

- How can the nozzle geometry be adapted during the printing process in order to utilise the aforementioned influences?

#### 3.2 Design and manufacturing of nozzles

To systematically investigate the effect of nozzle geometry in SC3DP, different variations of nozzle designs were analysed. The nozzle outlet diameter  $d_o$  is varied between 10 and 30 mm. Here, the smallest outlet diameter is limited by the increasing risk of clogging during the printing process. The nozzle inlet diameter  $d_i$  is kept constant at 25 mm due to the connection to the upstream nozzle holder. This results in three different basic nozzle types:

- tapered to the nozzle outlet ( $d_o = 10, 15, 20$  mm),
- straight ( $d_o = 25$  mm) and
- widened to the nozzle outlet ( $d_o = 30$  mm).

In addition, three different nozzle lengths  $L$  (100, 150, 200 mm) were investigated for an outlet diameter of 20 mm. An overview of all nozzles is shown in Table 1.

All nozzles were additively manufactured by Fused Deposition Modelling (FDM). Polyethylene terephthalate modified with glycol (PETG) was chosen due to its high resistance towards water. To improve the interchangeability of the nozzles within the experimental investigations, a quick coupler was designed and manufactured. The coupler is mounted to the SC3DP end effector via clamping. The coupler is connected to the interchangeable nozzles with a threaded connection (M42). The experimental setup, as well as a schematic of the changeable nozzle, are presented in Fig. 3.

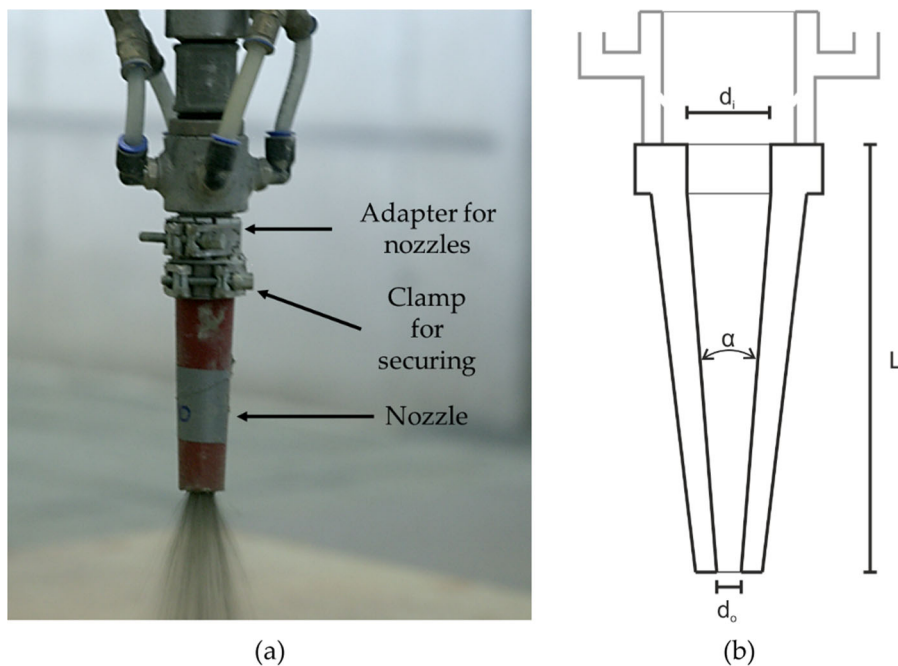


**Fig. 3** **a** Experimental setup connected to a robot during the process; **b** schematic of nozzle with relevant parameters: nozzle length ( $L$ ), nozzle inlet diameter ( $d_i$ ), nozzle outlet diameter ( $d_o$ ) and angle of nozzle ( $\alpha$ )

### 3.3 Specimen preparation

The tests were performed at the Digital Building Fabrication Laboratory (DBFL). The DBFL is a research facility funded by the German Research Foundation (DFG) for investigations on Digital Fabrication for construction processes. The facility consists of two independently movable gantry portals. One portal is mounted with an industrial robot (Stäubli TX200, Pfäffikon, Switzerland), resulting in 9 degrees of freedom (DOF) for processes such as SC3DP, while the other has a milling device mounted for supporting processes such as surface finishing with 5 DOF [6].

For the manufacturing of the specimens, a polymer-modified mortar with a maximum grain size of 2 mm (MC-Bauchemie GmbH Co., Bottrop, Germany) was used. The composition of the mortar is shown in Table 2.

The mortar was mixed in batches of 75 kg of dry material and 11.4 l of water using a pug mill mixer (Werner-Mader WM-Jetmix 125, Erbach, Germany). The mixing time was kept constant at 4 min. To ensure constant material quality, flow table tests (according to DIN EN 12350-5:2019-09 [20]) were performed during the experiments. A spread of

**Table 2** Mix composition of polymer-modified shotcrete mortar

Material	Content	Unit
Ordinary portland cement (OPC)	500	kg/m <sup>3</sup>
Pozzolan	160	kg/m <sup>3</sup>
Silica fume	25	kg/m <sup>3</sup>
Sand	1180	kg/m <sup>3</sup>
Pulverised additives and micro fibres	33	kg/m <sup>3</sup>

$f = 41 \text{ cm} \pm 6 \text{ cm}$  was observed. The material was then pumped through a 25 m hose (diameter = 35 mm) to the spray nozzle using a screw pump (Werner-Mader WM Variojet FU, Erbach, Germany). For each nozzle, 1.1 m long straight specimens consisting of 14 layers were manufactured. The process parameters chosen for the experimental investigations are shown in Table 3.

All specimens were stored in the DBFL workspace (at approximately 20 °C room temperature) for 1 day, covered with plastic foil to reduce the water loss by evaporation. Thereafter the specimens were placed for 27 days in a climate-controlled room at 20 °C and 65%

**Table 3** Process parameters for specimen production

Parameter	Value	Unit
Concrete volume flow	0.4	m <sup>3</sup> /h
Air volume flow	40	m <sup>3</sup> /h
Traverse speed	4500	mm/min
Nozzle-to-strand distance	200	mm
Number of layers	14	(–)

rel. humidity. The nozzle-to-strand-distance, defined as the distance from the outlet of the nozzle to the substrate, was kept constant at 200 mm (see Fig. 4).

### 3.4 Methods

The effects of nozzle outlet diameter  $d_o$  and nozzle length  $L$  were investigated regarding their influence on the jet (Sect. 3.4.1), the strand geometry (Sect. 3.4.2) and the mechanical hardened state properties (Sect. 3.4.3). The following chapter shows the different inspection and evaluation methods used to analyse and process the results of the investigations.

#### 3.4.1 Visual inspection of shotcrete jet

A digital single lens reflex (DSLR)—camera is used for the visual inspection of the shotcrete jet. The jet angle and velocity are qualitatively evaluated by examining the recordings. The entire specimen manufacturing was evaluated. Individual representative frames were selected to show the different characteristics of each spray pattern.

#### 3.4.2 Investigations on strand geometry

In order to examine the strand geometry, the 360° endless rotational 2D laser-scanner presented by Lachmayer [9] is used (Keyence LJ-X 8400, accuracy in height: 5 µm, accuracy in width: 10 µm). After printing, the laser scanner is mounted to the robot to scan the surface of all specimens. The raw data obtained by the 2D-laser scanner is split into point clouds containing only the data of one specimen. Each point cloud is individually levelled using the mean value of the lowest 10% of measured  $z$ -Values to identify the building surface as zero level.

The methodology of the analysis is presented in Fig. 5. For the investigation of the geometry, only the

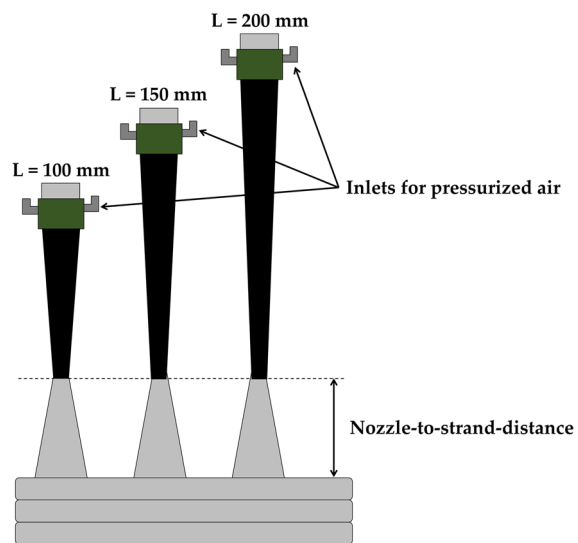


**Fig. 4** Visualisation of the used nozzle-to-strand-distance for the variation of nozzle length  $L$

middle section of each strand  $\pm 200$  mm is examined (Fig. 5a—left), as SC3DP printed specimen significantly flattens on the edges (see Fig. 5a—right) [9].

To calculate the width and height of each specimen, eight representative cross-sections, each 50 mm apart, are used. To reduce the influence of outliers by increasing the amount of points for the evaluation, two line measurements are joint for the evaluation (Fig. 5b). Due to a perpendicular orientation of the scanner to the printing direction and the build surface, the vast amount of measured points are either located close to the build surface ( $z = 0 \pm 10$  mm) or on top of the specimen ( $z > 80\%$  of  $z$ -maximum value), while the sides contain a low amount of points. For the investigation of width and height, only the data points of the top surface are relevant (see Fig. 5c).

The width of each area is determined by calculating the distance between the far most left and right point of the top surface. These points are determined by calculating  $y_{min}$  for the left side and  $y_{max}$  for the right side (see Fig. 5d). By using the top surface to calculate the strand width, narrower areas towards the bottom of the specimen cannot be measured. However, this limitation is not considered critical for the presented specimen geometry. To determine the specimen height of an area, the 95% quantile of all  $z$ -values inside the top surface is calculated. By doing so, the influence of potential outliers is reduced. In order to calculate the width and height of the entire

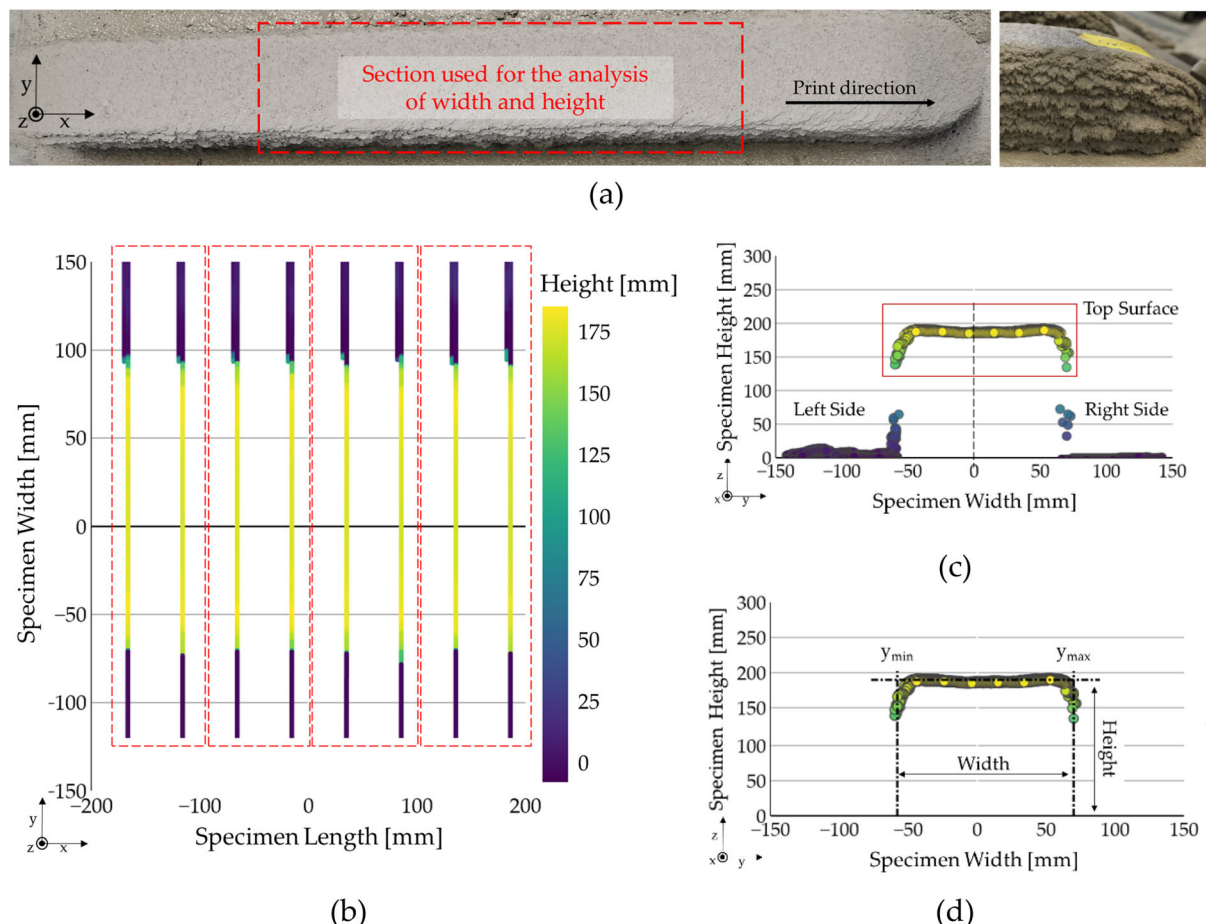


**Fig. 5** Methodology for the evaluation of the strand geometry showing **a** Test specimen for evaluation in top view; **b** 8 representative line measurements between the specimen, the mean value of all examined cross-sections is calculated.

#### 3.4.3 Investigations on mechanical properties

For mechanical testing, samples are sawn from the core of the manufactured strands, see Fig. 6a. Sawing is performed in the hardened state within 7 days before testing. All mechanical tests are carried out 28 days after manufacturing. Three prisms ( $160 \times 40 \times 40 \text{ mm}^3$ ) are sawn for the 3-point bending test according to DIN EN 196-1 [21]. For specimens that did not reach a height of 160 mm, prisms with a minimum length of 145 mm were also permitted for the 3-point bending test due to a support span of 100 mm. All specimens are tested parallel to the layer orientation with a centrally located interface (Fig. 6b). This allows to evaluate the

centre  $\pm 200 \text{ mm}$ ; **c** Side view of a cross-section with highlighted top surface; **d** Reduction of data from cross-section to calculate height and width

bond strength between the applied layers. In accordance with DIN EN 196-1 [21], compressive strength tests are performed on the end pieces of the sampled prisms (resulting in six specimens), also perpendicular to the layer orientation (Fig. 6c).

#### 3.5 Results and discussion

This chapter presents and discusses the results of the experiments. Similar to Sect. 3.4, the results are divided into three sections. First, the effect of varying nozzle geometry on the shotcrete jet is discussed (Sect. 3.5.1), followed by the changes in resulting strand geometry (Sect. 3.5.2). The discussion is concluded with an analysis of the mechanical properties, i.e. flexural strength and compressive strength (Section 3.5.3).

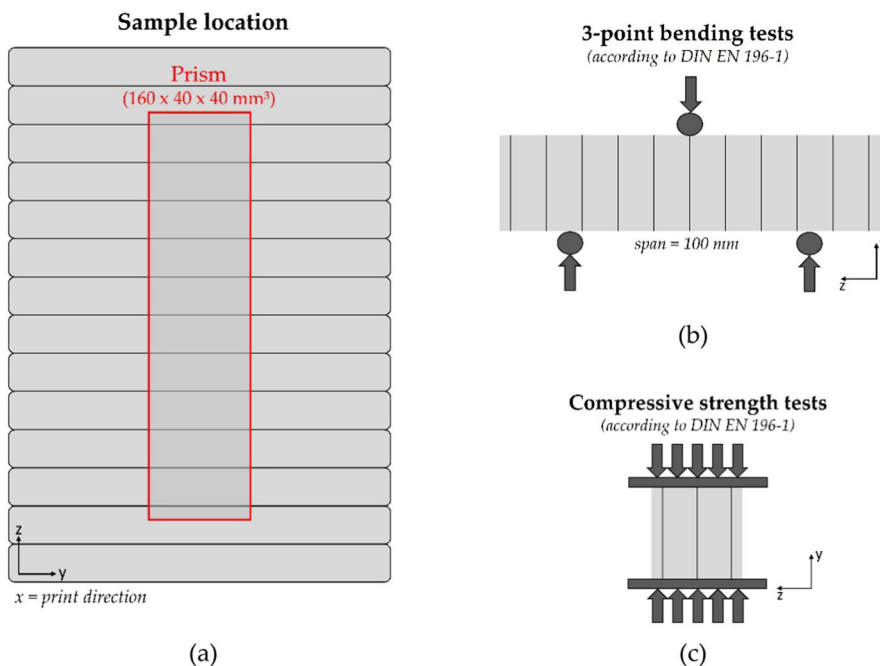


**Fig. 6** Mechanical testing of the manufactured specimens: **a** Location of sampling in the specimen cross-section, **b** test setup for 3-point bending tests, **c** Test setup for compressive

strength tests on the end pieces of the sampled prisms ( $y-z$ -cross section:  $40 \times 40 \text{ mm}^2$ )

### 3.5.1 Visual inspection of shotcrete jet and resulting strand surface

The results of the visual inspection are summarised in Fig. 7. The spray angle is similar for all nozzle outlet diameters. Regarding the jet velocity, a strong increase is observed as the outlet diameter decreases. Additionally, a more uniform and finer distribution of agglomerates is noticeable.

These results correspond to the basics of fluid mechanics and the continuity equation. While a constant air flow rate was used for the experiments and the nozzle angle  $\alpha$  was smaller than  $3^\circ$ , the same mass flow of air-agglomerate mixture inside the nozzle can be assumed [18]. While the nozzle inlet diameter is equal to the outlet diameter, the mass-flow rate remains constant. By decreasing the outlet diameter, the area of the nozzle outlet decreases, resulting in an increased velocity of the mass flow. Therefore, an increased jet velocity from a straight nozzle ( $d_o = 25 \text{ mm}$ ) to a tapered nozzle with a nozzle outlet diameter of  $d_o = 10 \text{ mm}$  is observed. Furthermore, finer agglomerates within the shotcrete jet at a

smaller outlet diameter might be related to the higher jet velocity. As the concrete enters the nozzle, it blocks the airflow. For smaller nozzle outlets, the pressure inside the nozzle increases faster, causing larger concrete agglomerates to accelerate and fragment into smaller particles, as the acceleration force is greater than the cohesion in larger particle agglomerations. The extent of splitting might correlate with the jet energy. Thus, smaller outlet diameters lead to smaller agglomerates in the jet.

For a variation in nozzle length, no visually noticeable change, neither in spray pattern nor in the velocity of the jet, is observed, although a longer nozzle could reduce the particle energy due to friction on the nozzle walls.

### 3.5.2 Investigations on strand geometry

The results of the investigations on the influences of the variation of nozzle outlet diameter and nozzle length on strand width and strand height are presented in the following section. A summary is shown in Table 4.

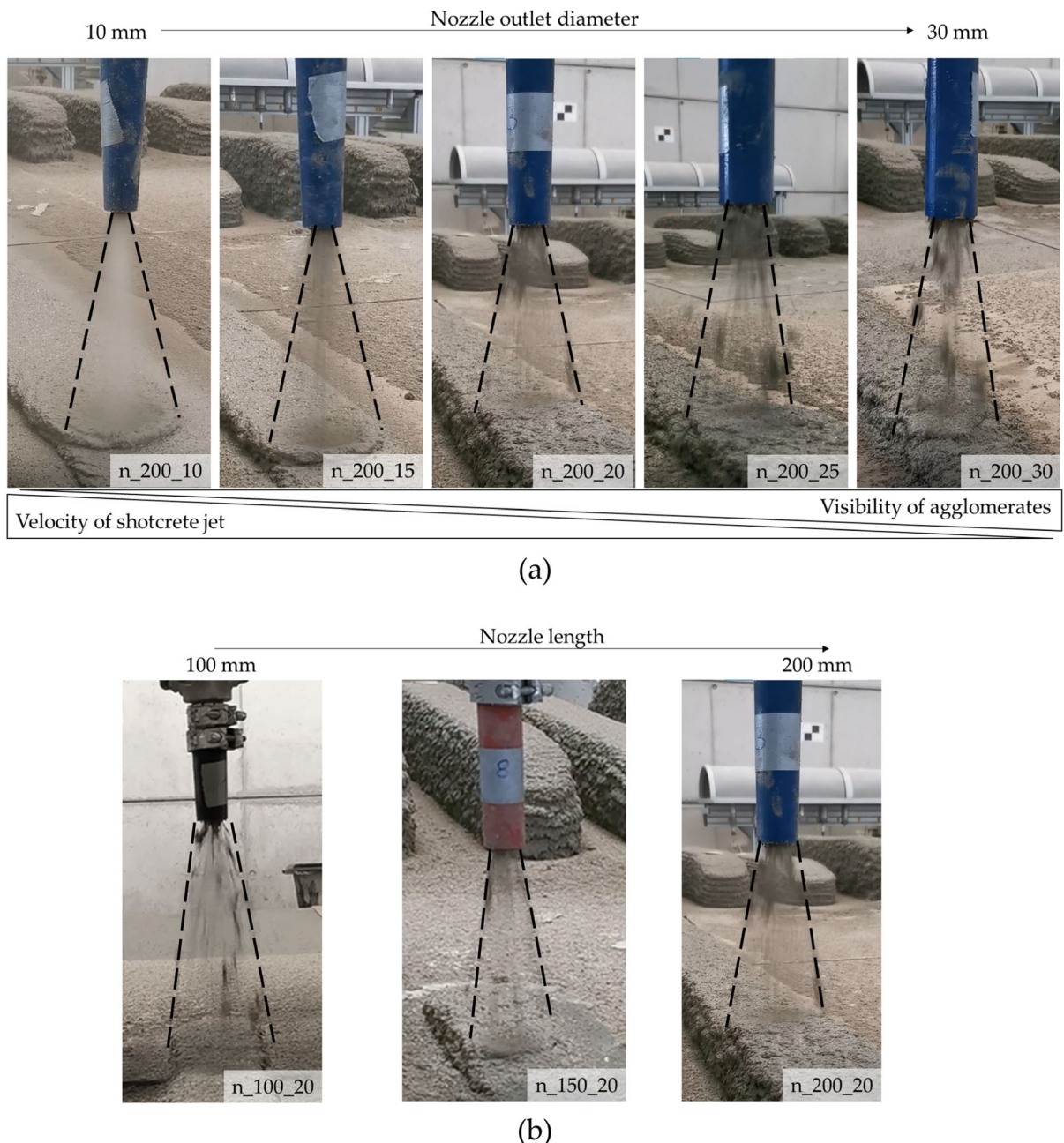


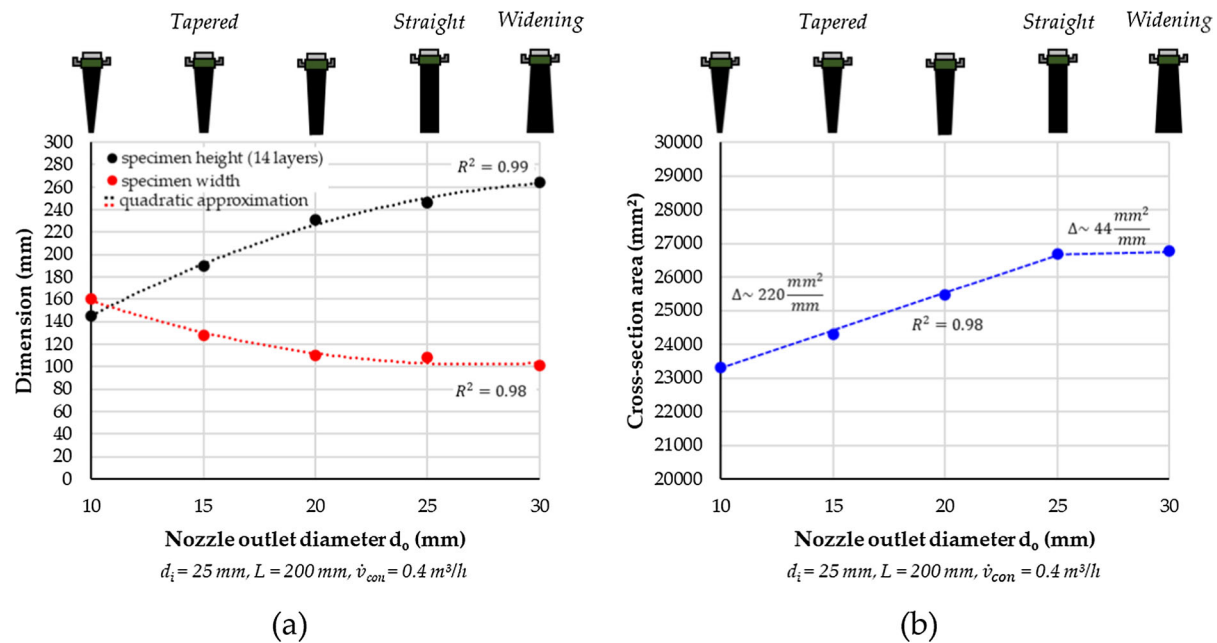
**Fig. 7** Visual inspection of shotcrete jets formed by **a** different nozzle outlet diameters and **b** different nozzle lengths

In general, a smaller nozzle outlet diameter leads to wider and lower strands, while for bigger diameters, the height increases and the width decreases, see Fig. 8. For further analysis, the results are plotted and approximated with an analytical model. A quadratic approximation shows high coefficients of determination for both the strand width ( $R^2 = 0.98$ ) and the

strand height ( $R^2 = 0.99$ ). Therefore, a strong influence of the nozzle outlet diameter on the strand geometry can be assumed. This might result from a higher impact velocity of the jet with decreasing outlet diameter. With a higher velocity, the sprayed concrete is pushed to the side, resulting in wider strands with smaller layer heights (Fig. 8a). In addition, the

**Table 4** Results of the nozzle geometry on the strand width and height (14 layers)

	Nozzle abbreviation	Strand height of 14 layers (mm)	Max strand width (mm)	Strand area ( $\text{mm}^2$ )
Nozzle outlet diameter	<i>n_200_10</i>	145.3	160.5	23,314.2
	<i>n_200_15</i>	189.9	128.0	24,307.9
	<i>n_200_20</i>	231.5	110.0	25,461.8
	<i>n_200_25</i>	246.0	108.5	26,685.3
	<i>n_200_30</i>	264.6	101.2	26,791.1
	$R^2$	0.99 (quadratic)	0.98 (quadratic)	0.98 (linear)
Nozzle length	<i>n_100_20</i>	221.4	105.9	23,449.4
	<i>n_150_20</i>	236.6	106.7	25,234.5
	<i>n_200_20</i>	231.5	110.0	25,461.8
	$R^2$	0.42 (linear)	0.88 (linear)	0.83 (linear)

**Fig. 8** Results on strand width and height for different **a** Nozzle outlet diameters and **b** calculated cross-section areas

increasing shear rate in the jet due to the higher jet velocities at small outlet diameters could lead to a reduction in the yield stress of the material, resulting in the aforementioned effect.

To determine the amount of deposited material, the cross-section area of each strand is evaluated (see Fig. 8b). The area is calculated by approximating the strand shape as a rectangle with straight edges, as presented in Fig. 5c. While the nozzle outlet diameter increases, the cross-section area increases proportionally. A linear correlation of around  $220 \text{ mm}^2$  (cross-

section area) per mm (nozzle outlet diameter) is observed. For the widening nozzle ( $d_200\_30$ ), only a minor increase of  $44 \text{ mm}^2/\text{mm}$  in comparison to the straight nozzle ( $d_200\_25$ ) is noted. Similar to the observed results for the strand width and height, this might result from a higher impact velocity of agglomerate-air mixture with a decreasing outlet diameter. A higher velocity increases the rebound of the sprayed material, which leads to a decrease in the strand cross-section.

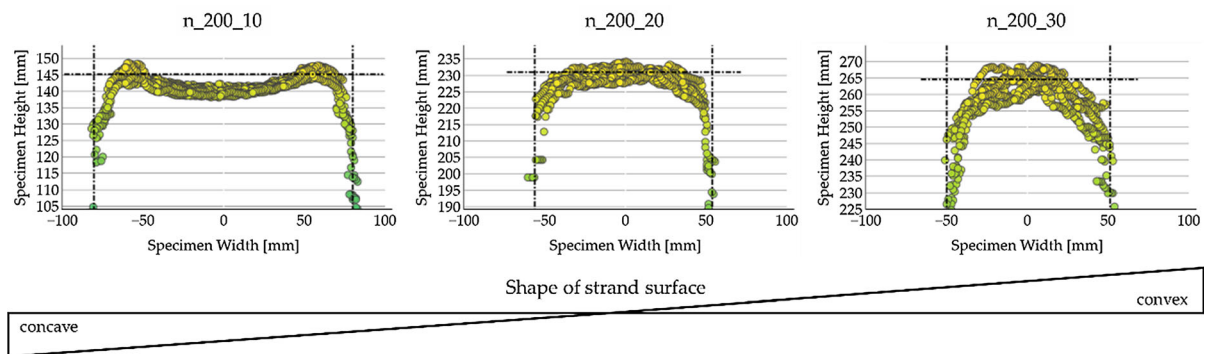


**Fig. 9** Detailed view of surface shape for different nozzle outlet diameters

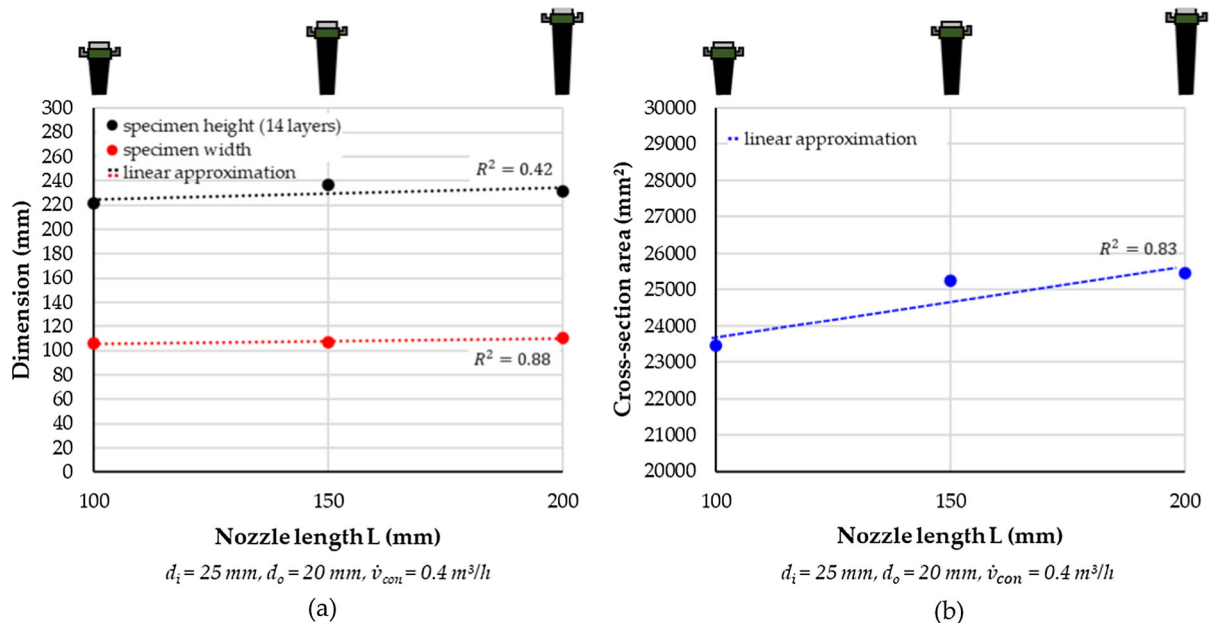


**Fig. 10** Results on **a** strand width and height for different Nozzle lengths and **b** calculated cross-section areas

The high influence of the jet velocity is further visible in the shape of the strand top surface. As seen in Fig. 9, the shape of the surface changes from concave at a small outlet diameter to convex at a big diameter. Because of the smaller outlet diameter and, therefore, higher impact energy of the aggregate, the material in already applied layers is deformed, resulting in lower layer heights and wider strands.

For a variation of nozzle lengths, only a minor influence of the parameter on strand width and height is observed. As the length increases from 100 to 200 mm, the strand width slightly increases from 105.9 to 110.0 mm with a linear correlation factor of

0.88. For the height, changing from 221.4 mm at  $L = 100 \text{ mm}$  to 231.5 mm at  $L = 200 \text{ mm}$ ,  $R^2$  is equal to 0.42 (Fig. 10a and Table 4). The cross-section increases from  $23449.4 \text{ mm}^2$  for  $L = 100 \text{ mm}$  to  $25461.8 \text{ mm}^2$  for  $L = 200 \text{ mm}$  with  $R^2 = 0.83$  (Fig. 10 b). These observations might be a result of reduced jet energy due to increased friction in longer nozzles.

### 3.5.3 Investigations on mechanical properties

Figure 11 shows the results of the mechanical tests for the investigated nozzle outlet diameters. The highest

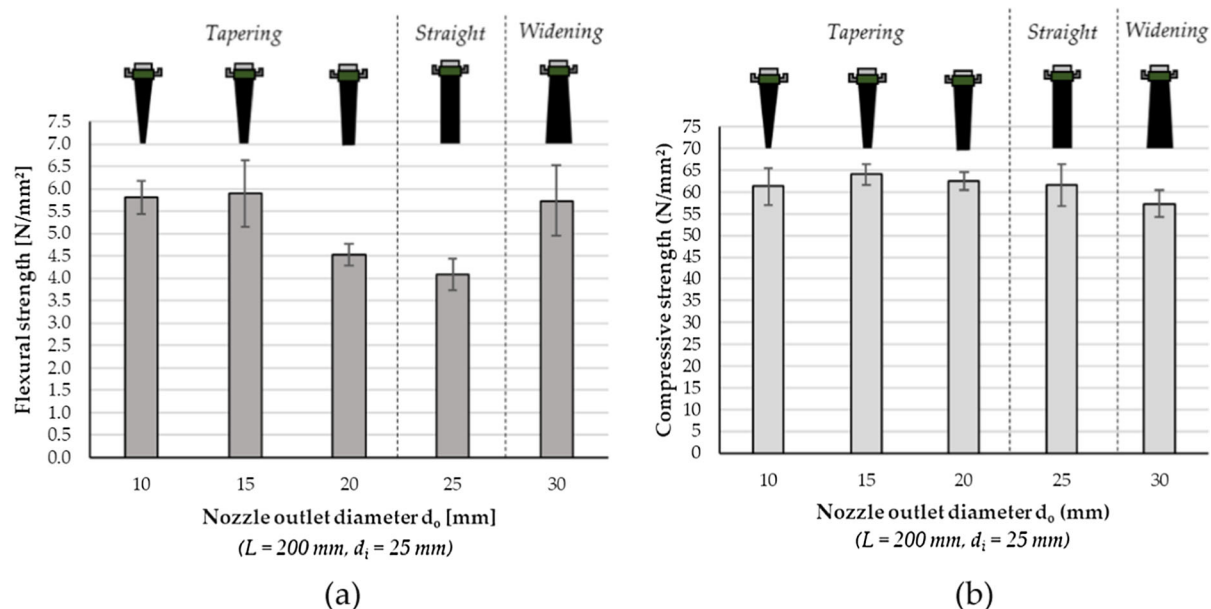


**Fig. 11** Results of **a** 3-point bending tests and **b** Compressive strength tests for different nozzle outlet diameters  $d_o$

flexural strengths of 5.80 and 5.89 N/mm<sup>2</sup> were obtained for the tapered nozzles at small nozzle diameters (10 and 15 mm). An increase in  $d_o$  to 20 mm resulted in a 23% reduction in flexural strength to 4.53 N/mm<sup>2</sup> compared to  $d_o = 15$  mm. A further increase in outlet diameter to a straight nozzle ( $d_o = 25$  mm) resulted in a further reduction in flexural strength to 4.08 N/mm<sup>2</sup>, representing the lowest average flexural strength. The observed decrease in layer bonding with increasing outlet diameter could be related to the decrease in sprayed concrete jet velocity. It can be assumed that the material applied with a small outlet diameter experienced greater compaction. Contrary to the observed trend, the widening nozzle ( $d_o = 30$  mm) shows an increase in flexural strength. This may be a result of the application of the material in larger agglomerates combined with a lower jet velocity resulting in higher interface tortuosity between the applied layers, which was investigated as being beneficial for the resulting layer bond strength [11]. Although the use of a widening nozzle ( $d_o = 30$  mm) results in advantageous mechanical properties, it should not be favoured for unrestricted use in SC3DP due to the low shotcrete velocity limiting the number of spray angles.

Figure 11b shows the results of the compressive strength tests for different outlet diameters. The highest compressive strength is 64.0 N/mm<sup>2</sup> for

$d_o = 15$  mm, and the lowest result is 57.3 N/mm<sup>2</sup> for  $d_o = 30$  mm. This can be attributed to the lower material compaction with decreasing jet velocity. However, considering the standard deviations, no significant trend can be identified.

Figure 12a shows the effect of nozzle length on the resulting flexural strength. All tests were carried out with an outlet diameter of 20 mm and, therefore, with a tapered nozzle. By shortening the nozzle from 200 to 100 mm, a 21% increase in flexural strength from 4.53 to 5.50 N/mm<sup>2</sup> is achieved. This could be explained by lower frictional losses within the nozzle and by the shorter distance of the pressurised air inlet to the substrate resulting in higher material compaction (see Fig. 4). However, for shorter nozzle lengths, a higher variation within flexural strength results is observed. The measured compressive strength ranges from 57.4 N/mm<sup>2</sup> ( $L = 150$  mm) to 62.55 N/mm<sup>2</sup> ( $L = 100$  mm and  $L = 200$  mm), see Fig. 12b. No clear effect of nozzle length on the resulting compressive strength can be observed.

#### 4 Design and experimental validation of an automated flexible SC3DP nozzle

Based on the previously presented results, the nozzle outlet diameter shows potential for in-situ control of

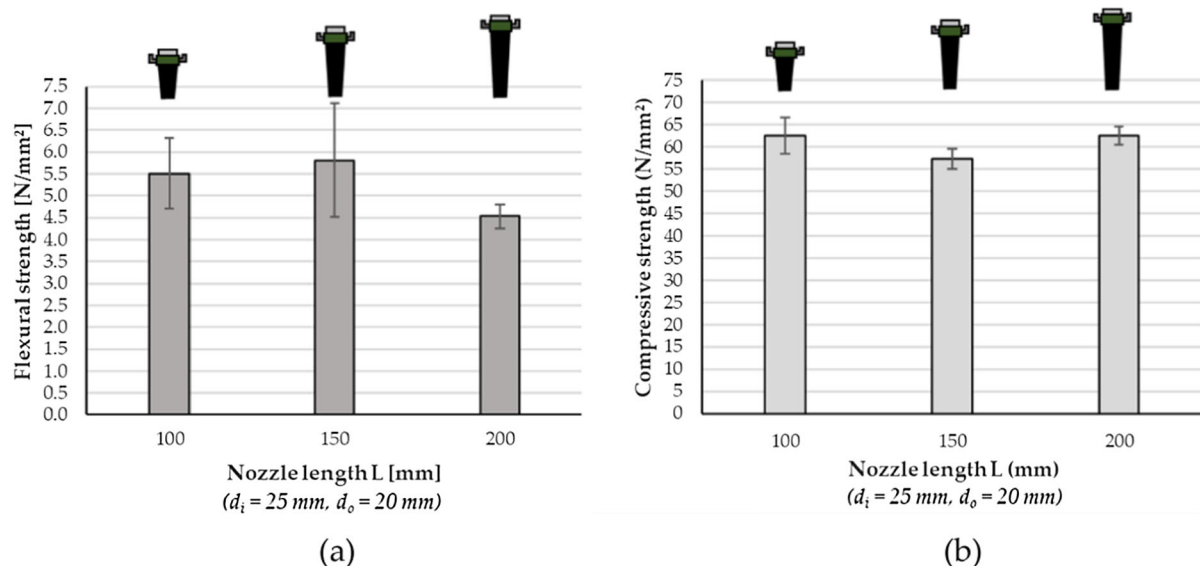


**Fig. 12** Results of **a** 3-point bending tests and **b** Compressive strength tests for different nozzle lengths  $L$

the strand geometry during SC3DP. Therefore, an adaptive SC3DP nozzle is developed to change the nozzle outlet diameter during the printing process. First, a literature and patent review is conducted to identify various solutions from other processes, such as concrete or plastic material extrusion (MEX), spray processes, such as spray painting, or other mechanisms used to change circular hole diameters. The identified mechanisms are evaluated against previously defined requirements before the most promising ones are built and tested for the SC3DP process.

#### 4.1 Concepts from patents and literature review

In extrusion processes, an adaptive nozzle system with a square geometry has already been examined. The nozzle diameter can be varied continuously until 25 mm [22]. A similar design is presented by Lao [23]. Other designs, such as variable scroll nozzles or iris-diaphragm-shaped nozzles, which are actuated in a rotary motion, are discussed in [24]. As another possibility, a vertical motion of different nozzle inserts can be used, which allows for a discrete adaption of the outlet diameter by raising or lowering a certain nozzle with the desired diameter [25]. A further solution is proposed as a segmented nozzle actuated by a lever [26]. Another concept for a star-shaped nozzle design with flexible material as a basis is presented by Mossberg [27]. In addition to the designs and

mechanisms previously mentioned, multi-nozzle devices are used, especially in MEX for plastics [28, 29] (Fig. 13).

To develop an adaptive nozzle system for SC3DP, these concepts are analysed and evaluated regarding the usability and applicability for the process. Special attention is given to the fact that for SC3DP, the material is accelerated by pressurised air in contrast to MEX. To ensure a good and non-obstructed air flow, sharp edges were removed during the design process. Further, widenings and dead spaces were minimised to reduce pressure loss. In order to realise the potential of this mechanism for complex printing shapes, a nozzle device with the capability of changing the outlet diameter continuously is preferred to a device with many nozzles of a constant outlet diameter or one nozzle with a mechanism for changing its outlet diameter in discrete steps. The result is an adoption of the scroll nozzle concept presented by [24] (see Fig. 14).

By rotating the disc located at the nozzle outlet, the cables tighten around the sheet metal, which narrows the outlet diameter. By rotating the disc counterclockwise, the cables are released, and the nozzle opens up due to the elasticity of the 0.2 mm thick sheet metal (1.4310) and the air pressure. This leads to a design for a flexible nozzle system with a length of 200 mm and a continuously changeable nozzle outlet diameter of 25–10 mm. At a rotation angle of 0°, the nozzle is

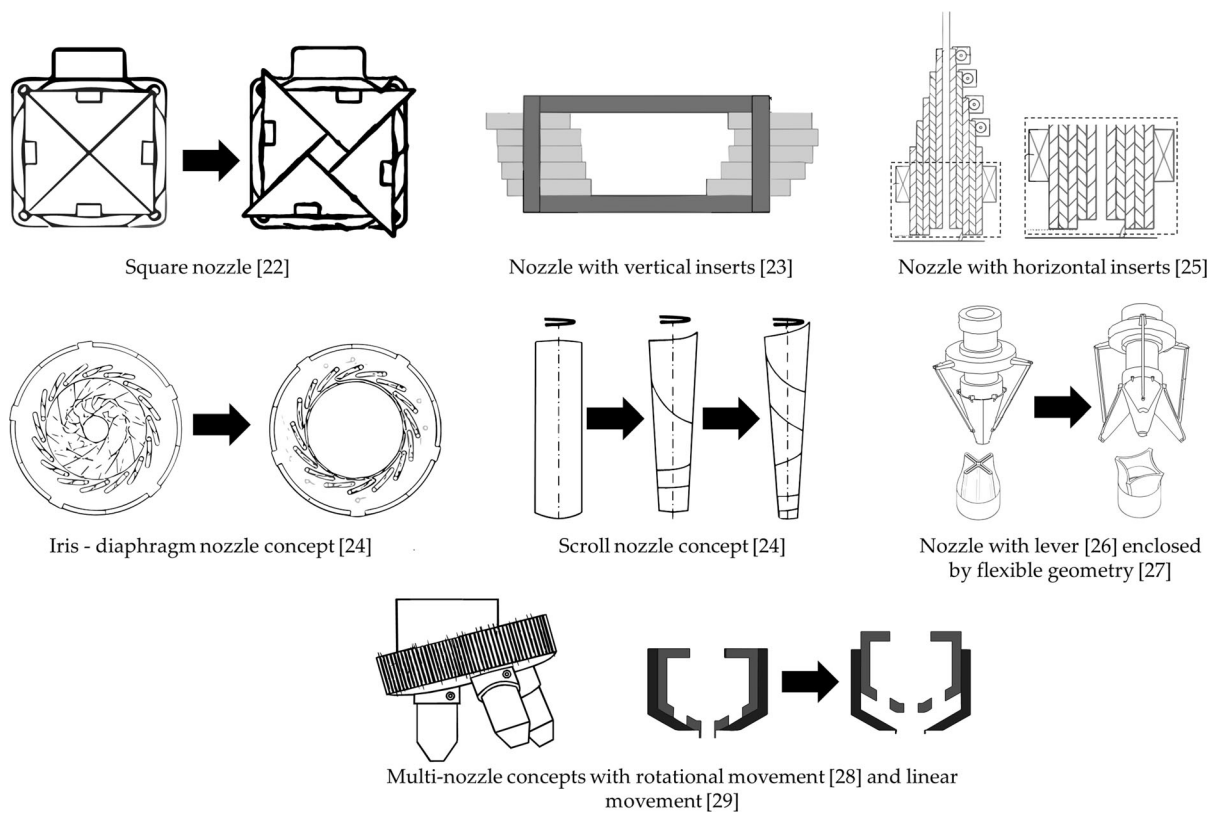


**Fig. 13** Various variable nozzle concepts from patents and publications [22–29]

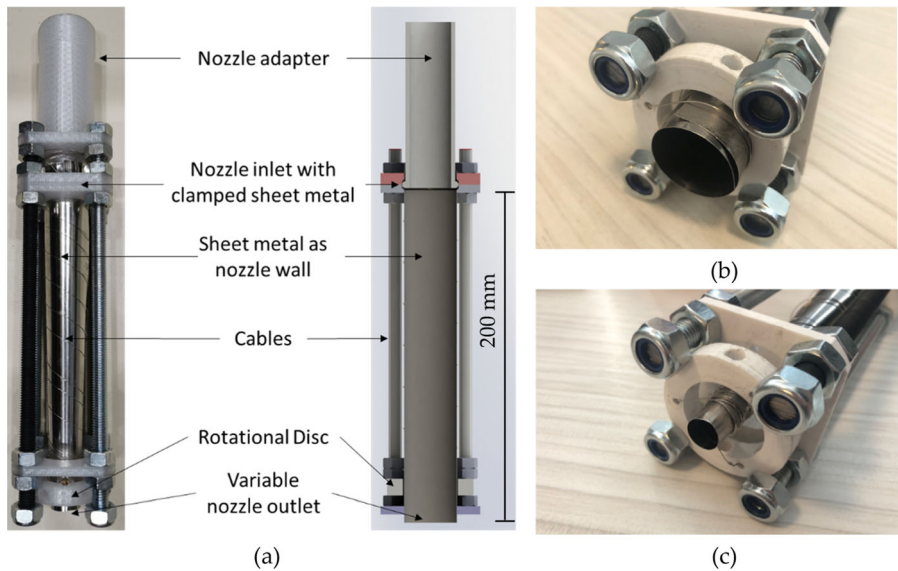


**Fig. 14** Flexible nozzle for SC3DP; **a** Side view and section view of nozzle prototype; **b** nozzle prototype with  $d_o = 25$  mm; **c** Nozzle prototype with  $d_o = 10$  mm

**Table 5** Correlation of rotation angle and nozzle outlet diameter

Angle (°)	0	120	240	360	480	600	720	840	960	1080	1200
Outlet diameter (mm)	25	23	20.7	18.5	16.8	15.2	13.9	12.9	11.9	10.9	10

fully opened. With an increasing rotation angle, the nozzle outlet diameter decreases, as seen in Table 5.

#### 4.2 Experimental validation

For the validation of the nozzle prototype, a 1 m long strand is printed with increasing the nozzle outlet diameter in three steps: 10, 15, and 20 mm. The nozzle outlet diameter is changed manually by rotating the disc connected to sheet metal, forming the nozzle outlet to 240° for a 20 mm outlet diameter, 600° for 15 mm and 1200° for a 10 mm outlet diameter. As seen in Fig. 15a, a variation of the outlet diameter changes the spray characteristic, similar to the results discussed in Sect. 3.4. By decreasing the nozzle diameter, an increase in the jet velocity (Sect. 3.4.1) and wider strands is achieved (Sect. 3.4.2). By increasing the nozzle outlet diameter from 10 to 20 mm, the strand width decreases by approximately 20% from 118.1 to 93.8 mm. Comparing this to the results presented in Sect. 3.5.2 with static nozzles, a decrease from 160.5 to 110.0 mm ( $\sim 31.3\%$ ) is

observed by a reduction of the outlet diameters from 10 to 20 mm (see Table 4).

As seen in Fig. 15a, the difference of 160 mm with a static nozzle and 118 mm with the variable nozzle might result from air leakage, reducing the jet velocity. By tightening the cables and thereby decreasing the nozzle outlet, the sheet metal deforms, and gaps with growing dimensions start to occur. Another reason for the different results might be the manual motion to decrease the nozzle outlet diameter.

Despite these potential shortcomings of this first prototype, this experimental validation proves the potential of a flexible nozzle system for changing the strand geometry during printing. Especially for building components with varying thickness, a single nozzle system with a variable nozzle outlet diameter expands the potential of using shotcrete-based AM.

#### 5 Conclusions and outlook

In the present study, the effects of nozzle outlet diameter and nozzle length on the resulting strand

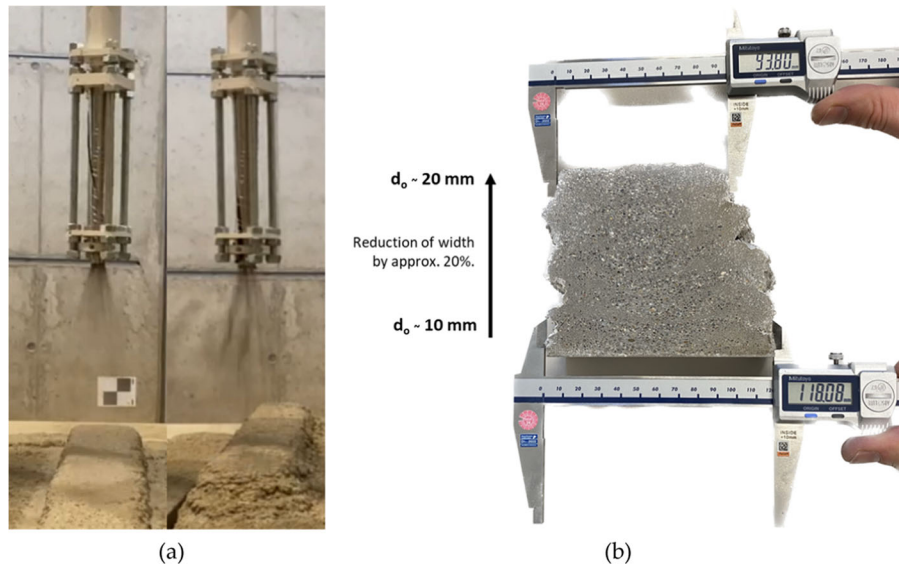


**Fig. 15** Validation of flexible nozzle; **a** Strands printed with  $d_o = 10 \text{ mm}$  and  $d_o = 20 \text{ mm}$ ; **b** manual measurement of cross-section

properties in SC3DP were investigated. In addition to the strand geometry (height, width), the influence on the hardened concrete properties, i.e. flexural strength, and compressive strength, were examined. The following results were obtained:

- The variation of the nozzle outlet diameter has a large influence on the velocity of the spray jet. Here, an increasing jet velocity can be observed with decreasing outlet diameter.
- The geometry of the produced strands is significantly affected by the nozzle outlet diameter. Decreasing the outlet diameters results in wider and flatter strands.
- For tapered and straight nozzle geometries, the layer bond strength is negatively affected by increased outlet diameters. However, the widened nozzle geometry counteracted this trend, resulting in an increased layer bond strength.
- Variations of the nozzle length in the investigated range (100–200 mm) show no significant effect on the resulting strand properties.
- A prototype for an automated, flexible nozzle was designed to change the nozzle outlet diameter during printing. The experimental validation demonstrated its functionality. Experiments with a gradually reduced outlet diameter were performed, showing similar behaviour regarding the influences on the layer geometry as the tested static nozzle outlet diameters.

The presented study shows that the specific control of the nozzle geometry is a well-suited process parameter for controlling component geometry and layer bonding in the SC3DP process. In order to better understand the observed effects of nozzle geometry on the resulting flexural strength, further research should include detailed investigations of the resulting material properties, i.e. material density, porosity and layer homogeneity in terms of aggregate distribution. Furthermore, knowledge of the effects of a varying nozzle outlet diameter in combination with other process parameters (air volume flow, concrete volume flow, etc.), material parameters (accelerator dosage) or path-planning approaches (nozzle-to-strand distance, traverse speed) is required to explore the full potential and limits of this new control parameter to increase the controllability of SC3DP.

**Author Contributions** Conceptualisation, MD, NF, KD and DL; methodology, MD, NF, KD and DL; software, MD and NF; validation, MD and NF; formal analysis, MD and NF; investigation, MD and NF; Provision of study materials, reagents, materials, patients, laboratory samples, animals, instrumentation, computing resources, or other analysis tools, KD and DL; data curation, MD and NF; writing—original draft preparation, MD and NF; writing—review and editing, MD, NF, KD and DL; visualisation, MD and NF; supervision, KD and DL; project administration, KD and DL; funding acquisition, KD and DL. All authors have read and agreed to the published version of the manuscript.

**Funding** Open Access funding enabled and organized by Projekt DEAL. Funded by the Deutsche Forschungsgemeinschaft (DFG, German Research Foundation)—TRR 277/1 2020—Project number 414265976. The authors thank the DFG for the support within the CRC/Transregio 277—Additive Manufacturing Construction (Project A04).

## Declarations

**Conflict of interest** The authors declare no conflict of interest.

**Open Access** This article is licensed under a Creative Commons Attribution 4.0 International License, which permits use, sharing, adaptation, distribution and reproduction in any medium or format, as long as you give appropriate credit to the original author(s) and the source, provide a link to the Creative Commons licence, and indicate if changes were made. The images or other third party material in this article are included in the article's Creative Commons licence, unless indicated otherwise in a credit line to the material. If material is not included in the article's Creative Commons licence and your intended use is not permitted by statutory regulation or exceeds the permitted use, you will need to obtain permission directly from the copyright holder. To view a copy of this licence, visit <http://creativecommons.org/licenses/by/4.0/>.

## References

1. Bos F, Wolfs R, Ahmed Z, Salet T (2016) Additive manufacturing of concrete in construction: potentials and challenges of 3D concrete printing. *Virtual Phys Prototyp* 11:209–225
2. Roussel N (2018) Rheological requirements for printable concretes. *Cem Concr Res* 112:76–85
3. Buswell RA, Bos FP, Da Silva WRL, Hack N, Kloft H, Lowke D, Freund N, Fromm A, Dini E, Wangler T et al (2022) Digital fabrication with cement-based materials: process classification and case studies. In: Roussel N, Lowke D (eds) *Digital fabrication with cement-based materials*. Springer, Cham, pp 11–48.
4. Lowke D, Mai I, Keita E, Perrot A, Weger D, Gehlen C, Herding F, Zuo W, Roussel N (2022) Material-process interactions in particle bed 3D printing and the underlying physics. *Cem Concr Res* 156:106748

5. Mechtcherine V, Bos FP, Perrot A, da Silva WL, Nerella VN, Fataei S, Wolfs R, Sonebi M, Roussel N (2020) Extrusion-based additive manufacturing with cement-based materials—production steps, processes, and their underlying physics: a review. *Cem Concr Res* 132:106037
6. Hack N, Kloft H (2020) Shotcrete 3D printing technology for the fabrication of slender fully reinforced freeform concrete elements with high surface quality: a real-scale demonstrator. In: Bos FP, Lucas SS, Wolfs RJ, Salet TA (eds) Second RILEM international conference on concrete and digital fabrication. Springer, Cham, pp 1128–1137.
7. Liu X, Li Q, Li J (2022) Shrinkage and mechanical properties optimisation of spray-based 3D printed concrete by PVA fiber. *Mater Lett* 319:132253
8. Wangler T, Pileggi R, Gürel S, Flatt RJ (2022) A chemical process engineering look at digital concrete processes: critical step design, inline mixing, and scaleup. *Cem Concr Res* 155:106782
9. Lachmayer L, Böhler D, Freund N, Mai I, Lowke D, Raatz A (2023) Modelling the influence of material and process parameters on Shotcrete 3D Printed strands - cross-section adjustment for automatic robotic manufacturing. *Autom Constr* 145:104626
10. Dreßler I, Freund N, Lowke D (2020) Control of strand properties produced with Shotcrete 3D Printing by accelerator dosage and process parameters. In: Digital Concrete 2020—2nd RILEM International Conference on Concrete and Digital Fabrication **2020**.
11. Dreßler I, Freund N, Lowke D (2020) effect of accelerator dosage on fresh concrete properties and on interlayer strength in shotcrete 3D printing. In: Materials Journal, Special Issue “Concrete 3D Printing and Digitally-Aided Fabrication”.
12. Buswell RA, da Silva WL, Bos FP, Schipper HR, Lowke D, Hack N, Kloft H, Mechtcherine V, Wangler T, Roussel N (2020) A process classification framework for defining and describing Digital Fabrication with Concrete. *Cem Concr Res* 134:106068
13. Kloft H, Krauss H-W, Hack N, Herrmann E, Neudecker S, Varady PA, Lowke D (2020) Influence of process parameters on the interlayer bond strength of concrete elements additive manufactured by Shotcrete 3D Printing (SC3DP). *Cem Concr Res* 134:106078
14. Böhler D, Mai I, Freund N, Lachmayer L, Raatz A, Lowke D (2022) Influence of material and process parameters on hardened state properties of shotcrete 3D-printed elements. In: Buswell R, Blanco A, Cavalaro S, Kinnell P (eds) Third RILEM international conference on concrete and digital fabrication. Springer, Cham, pp 255–260.
15. Lu B, Li M, Wong TN, Qian S (2021) Effect of printing parameters on material distribution in spray-based 3D concrete printing (S-3DCP). *Autom Constr* 124:103570
16. Nolte N, Heidmann-Ruhz M, Krauss H-W, Budelmann H, Wolter A (2018) Entwicklung von Spritzbetonrezepturen mit steuerbaren Eigenschaften für die robotergestützte additive Fertigung von Betonbauteilen. Spritzbeton-Tagung 2018, Tagungsband der 12. Fachtagung in Alpbach.
17. Krause M, Otto J, Bulgakov A, Sayfeddine D (2018) Strategic optimization of 3D-concrete-printing using the method of CONPrint3D®. In: Buswell R, Blanco A, Cavalaro S, Kinnell P (eds) Proceedings of the 35th International symposium on automation and robotics in construction (ISARC). International Association for Automation and Robotics in Construction (IAARC).
18. Petit A, Stucki W, Lullin S, Galé B, Zuliani F (2021) Econcrete structure manufacturing apparatus and method: European Patent Specification.
19. Galé B, Ursenbacher T, Petit A, Bourquin V (2022) Shotcrete 3DCP projection angle and speed optimisation: experimental approaches and theoretical modelling. In: Buswell R, Blanco A, Cavalaro S, Kinnell P (eds) Third RILEM international conference on concrete and digital fabrication. Springer, Cham, pp. 261–266.
20. DIN EN 12350-5:2019-09, Prüfung von Frischbeton – Teil\_5: Ausbreitmaß; Deutsche Fassung EN\_12350-5:2019; Beuth Verlag GmbH: Berlin.
21. Deutsches Institut für Normung (DIN). DIN EN 196-1:2016-11: Methods of testing cement - Part 1: Determination of strength; German; Beuth Verlag GmbH, 2016. Available online: <https://doi.org/10.31030/2482416>.
22. Xu J, Ding L, Cai L, Zhang L, Luo H, Qin W (2019) Volume-forming 3D concrete printing using a variable-size square nozzle. *Autom Constr* 104:95–106
23. Lao W, Li M, Tjahjowidodo T (2021) Variable-geometry nozzle for surface quality enhancement in 3D concrete printing. *Addit Manuf* 37:101638
24. Wan Q, Xu Y, Lu C (2018) A fundamental study of parameter adjustable additive manufacturing process based on FDM process. *MATEC Web Conf* 189:5001
25. Shin B, Hong T, Park C, Hong S, Kim M (2015) Nozzle having variable diameter for 3D printer and method for controlling the same(KR101725302B1). <https://patents.google.com/patent/KR101725302B1/en>
26. Fan Y (2019) Variable-caliber nozzle of 3D printer B29C 64/209(CN 211807880 U). <https://patentimages.storage.googleapis.com/7c/2a/ef92058ccf54f8cd/CN211807880U.pdf>
27. Moosberg M, Barbat AC (2021) A system with a dynamic variable size nozzle orifice for three-dimensional printing: U.S. Patent Application.
28. Brooks H, Lupeanu ME, Piorkowski B (2013) Research towards high speed extrusion freeforming. *IJRAPIDM* 3:154
29. Xiong G, Shen Z, Liu X, Wang F (2014) Multi-nozzle 3D printer and method for controlling speed and precision of multi-nozzle 3D printer(CN00010408511A). <http://www.casctcp.com/Files/upload/file/8ec79457b1581011a862.pdf>

**Publisher's Note** Springer Nature remains neutral with regard to jurisdictional claims in published maps and institutional affiliations.

